Available online at www.sciencedirect.com
SCIENCE DIRECT®
Tectonophysics 363 (2003) 1–18
TECTONOPHYSICS
www.elsevier.com/locate/tecto

Overprinting faulting mechanisms during the development of multiple fault sets in sandstone, Chimney Rock fault array, Utah, USA

Nicholas C. Davatzes*, Atilla Aydin, Peter Eichhubl

Department of Geological and Environmental Sciences, Stanford University, Stanford, CA 94305-2115, USA

Received 6 March 2002; accepted 1 November 2002

Abstract

The deformation mechanisms producing the Chimney Rock normal fault array (San Rafael Swell, Utah, USA) are identified from detailed analyses of the structural components of the faults and their architecture. Faults in this area occur in four sets with oppositely dipping fault pairs striking ENE and WNW. The ENE-striking faults initially developed by formation of deformation bands and associated slip surfaces (deformation mechanism 1). After deformation band formation ceased, three sets of regional joints developed. The oldest two sets of the regional joints, including the most prominent WNW-striking set, were sheared. Localized deformation due to shearing of the WNW-striking regional joints formed WNW-striking map-scale normal faults. The formation mechanism of these faults can be characterized by the shearing of joints that produces splay joints, breccia, and eventually a core of fault rock (deformation mechanism 2). During this second phase of faulting, the ENE-striking faults were reactivated by shear across the slip surfaces and shearing of ENE-striking joints, producing localized splay joints and breccia (similar to deformation mechanism 2) superimposed onto a dense zone of deformation bands from the first phase. We found that new structural components are added to a fault zone as a function of increasing offset for both deformation mechanisms. Conversely, we estimated the magnitude of slip partitioned by the two mechanisms using the fault architecture and the component structures. Our analyses demonstrate that faults in a single rock type and location, with similar length and offset, but forming at different times and under different loading conditions, can have fundamentally different fault architecture. The impact by each mechanism on petrophysical properties of the fault is different. Deformation mechanism 1 produces deformations bands that can act as fluid baffles, whereas deformation mechanism 2 results in networks of joints and breccia that can act as preferred fluid conduits. Consequently, a detailed analysis of fault architecture is essential for establishing an accurate tectonic history, deformation path, and hydraulic properties of a faulted terrain.

Keywords: Deformation band; Joint; Sheared joint; Faulting mechanism; Fault architecture

1. Introduction

Two distinct mechanisms of fault formation in sandstone have been described: (1) faults formed by deformation bands and (2) faults formed by formation

* Corresponding author.
E-mail addresses: davatzes@pangea.stanford.edu (N.C. Davatzes), aydin@pangea.stanford.edu (A. Aydin), eichhubl@pangea.stanford.edu (P. Eichhubl).

0040-1951/02/$ - see front matter © 2002 Elsevier Science B.V. All rights reserved.
doi:10.1016/S0040-1951(02)00647-9

and subsequent shearing of joints (Aydin, 2000). Each mechanism produces a different set of structural components with a characteristic geometry and distribution resulting in distinctive fault architectures. Deformation bands are characterized by thin tabular zones of cataclasis in sandstone (Engelder, 1974; Aydin and Johnson, 1978; Antonellini et al., 1994) that accommodate millimeters to centimeters of offset (Fig. 1a). Faults composed of deformation bands accumulate offset by addition of new deformation bands to form an anastomosing zone of deformation bands. Eventually, a planar discontinuity forms along the zone of deformation bands providing a slip surface that accommodates the majority of subsequent offset. As the offset increases, so do the length and the number of slip surfaces. Thus, these faults are composed of three characteristic structures: (1) individual deformation bands, (2) zones of deformation bands, and (3) slip surfaces.

A second macroscopic deformation mechanism in sandstone is characterized by shearing of preexisting discontinuities such as joints or bedding interfaces. Shearing of joints results in local tension near the joint tips where new joints called *splay joints* may propagate (Cotterell and Rice, 1980; Segall and Pollard, 1983; Granier, 1985; Cruikshank et al., 1991). Splay joints have been identified in the literature as horsetail fractures (Granier, 1985), pinnate fractures (Engelder,

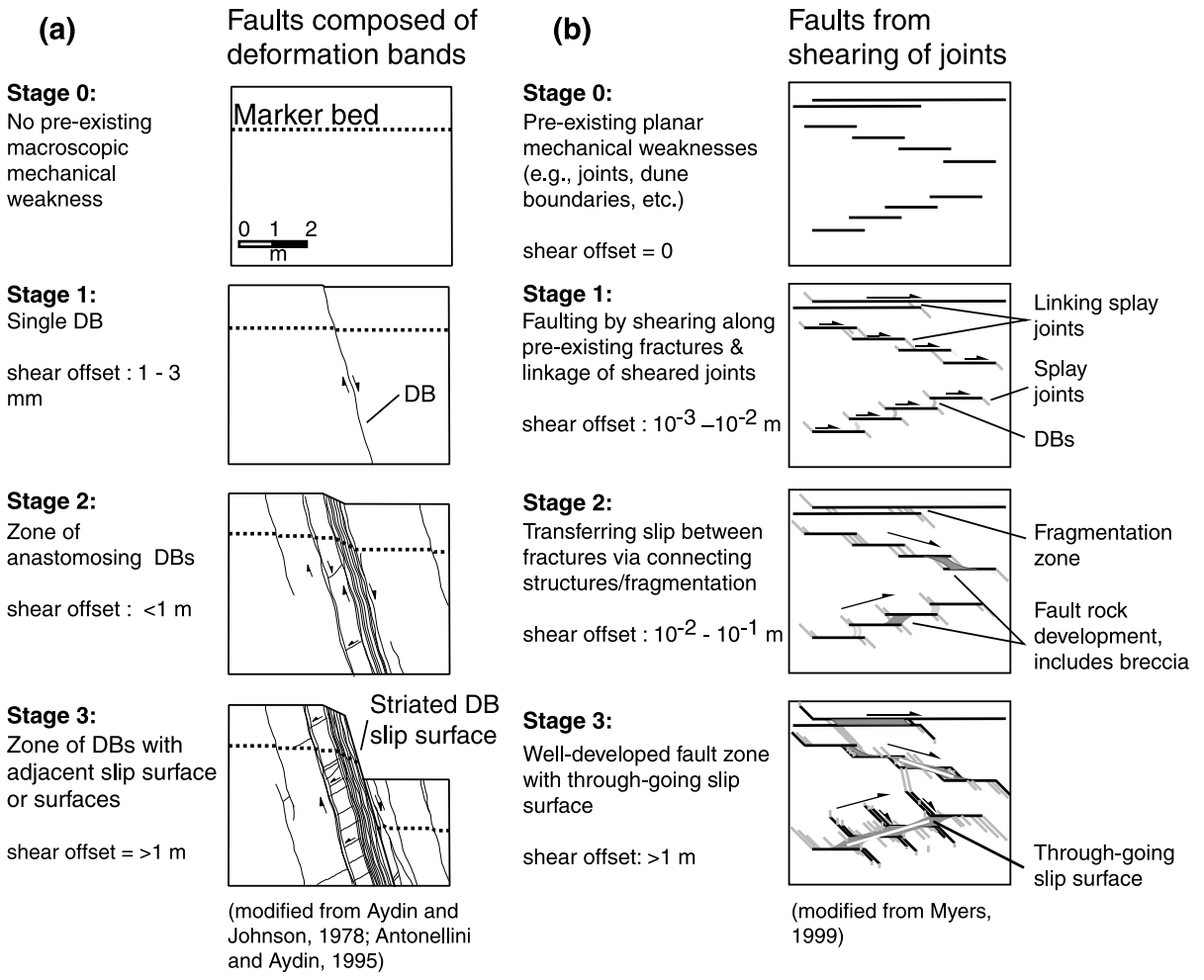

Fig. 1. Mechanisms of fault development in sandstone: (a) deformation banding (DB) and (b) jointing and subsequent shearing.

1987), splay fractures (Martel et al., 1988), splay cracks (Martel, 1990), kink fractures (Cruikshank et al., 1991), bridge cracks, and tail cracks (Cruikshank and Aydin, 1994). We adopt the term *splay joint* to emphasize that these structures are joints that form under specific circumstances and result in a characteristic geometry with respect to the sliding discontinuity. Segall and Pollard (1983) and Martel (1988) described joints that had been sheared and coalesced into a through-going fault by a system of splay joints in granodiorite. Myers (1999) documented the formation of zones of fragmentation, breccia, and fault rock by the formation of splay joints that connected sheared joints in en echelon or parallel arrays (Fig. 1b) in sandstone. As offset increases, early-formed splay joints can be reactivated in shear and form a second generation of splay joints (Myers, 1999). The orientation of faults that incorporate multiple sheared joints depends on how individual sheared joints are linked by splay joints (e.g., the three cases in Fig. 1b). Fault rock along this type of fault is characterized by white color, grain size reduction, poor consolidation, and is spatially associated with breccia and fragmentation. The characteristic structures of "joint-based faulting" include (1) joints (or other preexisting discontinuities, for example a slip surface), (2) sheared joints, (3) splay joints, (4) zones of fragmentation, and (5) fault rock (Myers, 1999).

The structural analysis of faulted terrains is commonly based on criteria including the length, height, offset, spacing, and orientation of faults and sets of faults (e.g., Anderson, 1951; Krantz, 1988; Barnett et al., 1989; Dawers and Anders, 1995; Schlische et al., 1996; Maerten, 2000). This type of analysis does not adequately address the relative timing of faults or properties of fault zones. We contend that a detailed analysis of faulting mechanisms and the resulting architecture complements a regional structural analysis that intends to reconstruct the tectonic history of a faulted terrain. Furthermore, we propose that recognizing fault architecture as the product of specific deformation mechanisms provides a basis for predicting fault zone characteristics such as the occurrence and distribution of joints, fragmented or brecciated rock, or deformation bands along a fault.

Fault orientations, spacing, and slip have been used to calculate the orientations and ratios of all three principal strains (Krantz, 1988). Without distinguishing phases of fault development, only the finite state of strain is represented. Similarly, distinguishing neoformed faults from faults reactivated during a subsequent phase of fault activity is integral for accurate stress inversion (Huang and Angelier, 1989) or for fault slip distribution analysis (Maerten, 2000). Whether a fault will act as fluid conduits or barriers might depend on the development and distribution of fault rock as well as the attendant structures like joints and deformation bands in the damage zone (Chester and Logan, 1986; Caine et al., 1996; Matthai et al., 1998; Knipe et al., 1998; Taylor et al., 1999; Aydin, 2000; Flodin et al., 2001). Hence, the architecture, temporal evolution, and overprinting relationships of faults are crucial for elucidating hydrocarbon migration pathways and potential traps.

This study examined the Chimney Rock fault system in the San Rafael Swell of Utah, USA to

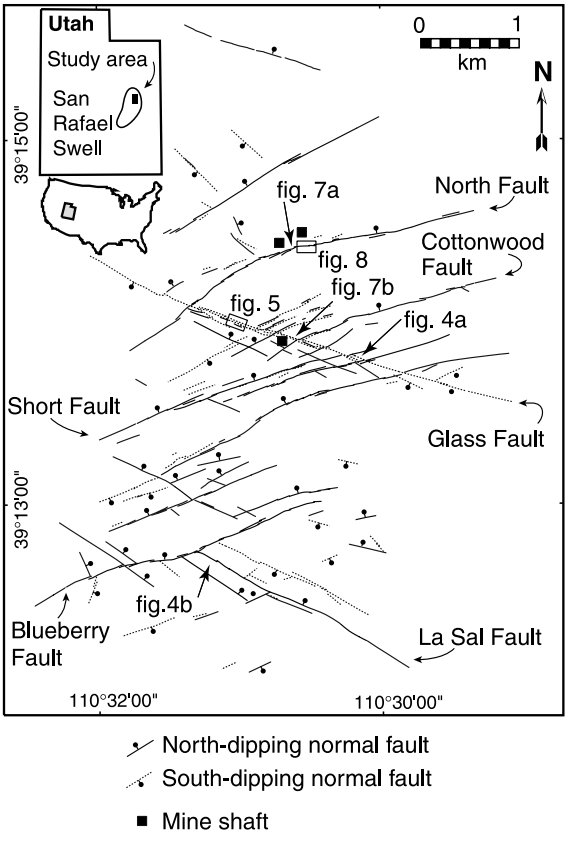

Fig. 2. Distribution of faults in the study area. Basic fault map was modified from Maerten (1999).

characterize deformation band and joint-based faulting styles in multiple fault sets in a single location and single rock type. We mapped the structural components of faults to distinguish different mechanisms of fault formation. Based on detailed mapping and analyses, we estimated the relative contribution of the structural products associated with each mechanism to faulting. The macroscopic deformation mechanisms provided a means to determine various phases of the formation and evolution of a normal fault system composed of multiple sets of faults in sandstone.

2. Geologic setting

The Chimney Rock normal fault system is located in $6 \pm 2^{\circ}$-dipping strata (Krantz, 1988) straddling the northern anticlinal axis of the San Rafael Swell of

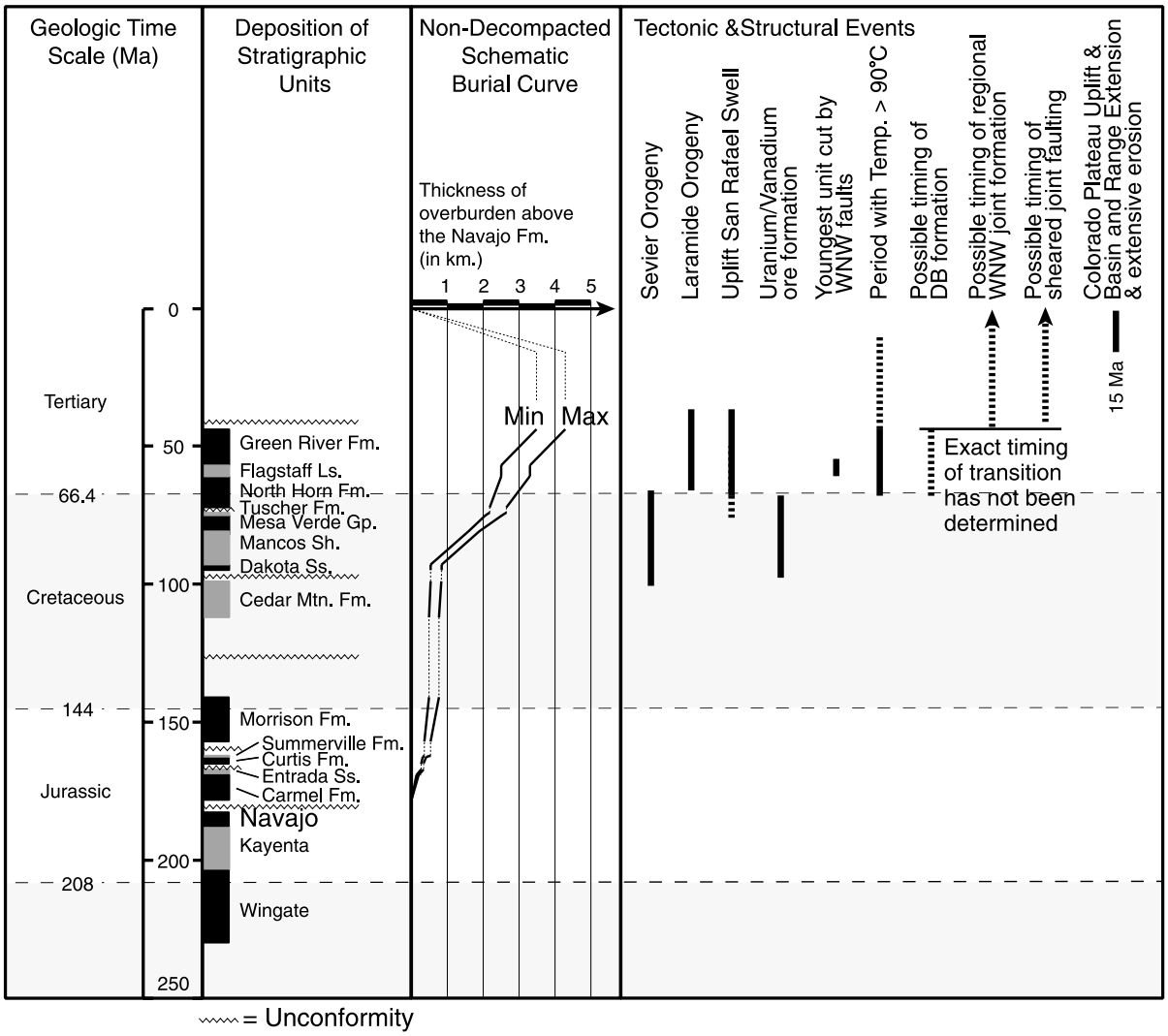

Fig. 3. Timing of events in the Chimney Rock area. Jagged lines during nondeposition of units are unconformities. The two curves represent maximum and minimum estimates of overburden thickness above the top of the Navajo Formation estimated by combining data from Hintze (1988) and Gilluly (1928). Units younger than Late Cretaceous are extrapolated from surrounding areas because they are eroded from the San Rafael Swell.

central Utah, USA (Fig. 2). The swell is a dome-like structure composed of a Phanerozoic sedimentary sequence (Kelley, 1955; Dickinson and Snyder, 1978). The normal fault system offsets Jurassic Navajo sandstone and overlying thinly bedded limestone, siltstone, and mudstone of the basal Carmel Formation. In the study area, the eolian Navajo sandstone is a well-sorted, cross-stratified, quartz arenite with 13–25% porosity (Shipton and Cowie, 2001). Navajo Formation thickness varies from 140–170 m (Gilluly, 1928; Gilluly and Reeside, 1928). The footwalls of faults up to 6 km long are exposed as scarps of resistant Navajo sandstone. Polished and striated fault surfaces along these scarps dip 55–90° (Krantz, 1989). Striations rake from 90–40°E and W (Maerten, 2000). Maximum vertical offset across a single fault in the entire study area is 38 m (Maerten, 2000; Maerten et al., 2001). Bedding plane exposure of Navajo sandstone along faults is primarily limited to the footwall and fault zones crossed by washes (Fig. 2).

Previous authors suggested that the timing of fault formation coincided with uplift of the San Rafael Swell during the Laramide orogeny between 66.4 and 37 Ma (Fig. 3) (Krantz, 1988; Maerten, 2000; Shipton and Cowie, 2001). The timing of uplift of the San Rafael Swell is constrained by changing alluvial architecture and thinning of the Price River Formation in the early Campanian (83.5–71.3 Ma) (Guiseppe and Heller, 1998). During this period, the minimum burial depth of the Navajo Formation was 2–4 km (Fig. 3). The lack of intact units younger than Late Cretaceous in the area does not allow reconstruction of a definitive maximum burial depth. Previous research at the Chimney Rock fault array in Utah has focused on geometric, kinematic, and mechanical characteristics of the fault array (Krantz, 1988; Cowie and Shipton, 1998; Maerten, 2000; Shipton and Cowie, 2001) but not on the occurrence and distribution of multiple faulting mechanisms.

3. Results

All exposed faults were examined for the occurrence, distribution, and relative timing of deformation mechanisms. The North and Glass faults (Fig. 2) were selected for detailed mapping to document and interpret deformation mechanisms because of excellent exposures. Locations isolated from fault intersections were chosen to minimize the impact of different fault sets on the occurrence, distribution, and orientations of struc-

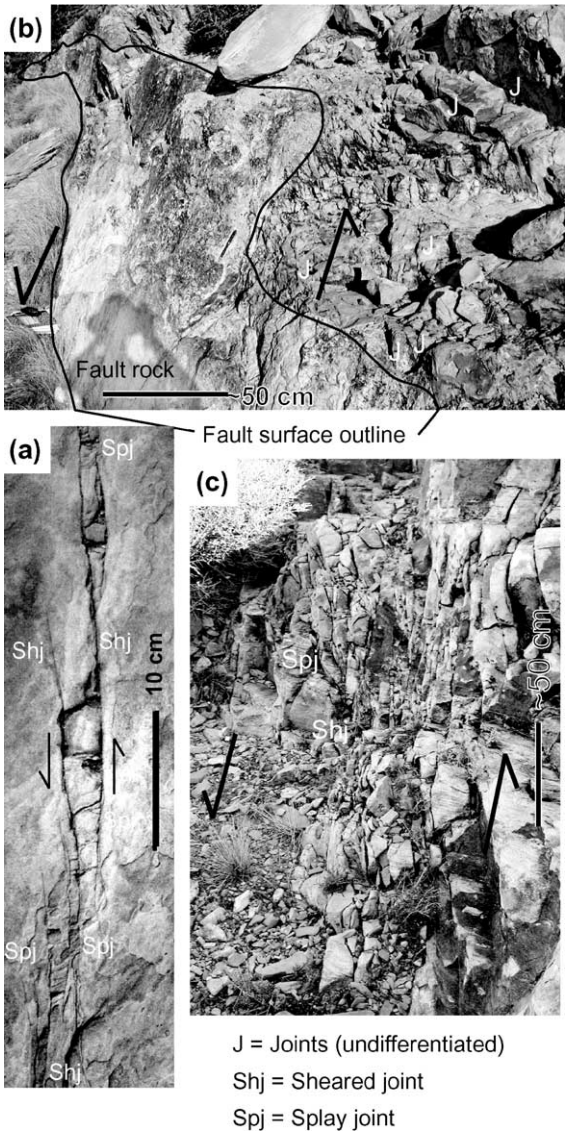

Fig. 4. Components of WNW-striking faults. (a) Splay joints resulting from slip on joints. Offset: 1 cm. (b) Well-developed breccia and fault rock adjacent to fault surface along Glass fault. Vertical offset 22 m. Fault rock along WNW-striking faults is characterized by white color, grain size reduction, poor consolidation, and is spatially associated with breccia and fragmentation. (c) Fragmentation and breccia zone along La Sal fault. Vertical offset 13 m. Several examples of each structural component are indicated in the photograph. Figure locations are indicated in Fig. 2.

tures. The Glass fault (Fig. 2) is a WNW-striking and SSW-dipping normal fault, with a maximum vertical offset of about 38 m. The North fault (Fig. 2) is an ENE-striking and NNW-dipping normal fault with a maximum vertical offset of about 28 m. Detailed maps were produced in the field on photographs obtained from a camera suspended below a helium weather balloon approximately 100 m above the outcrop (see Myers, 1999, for information about the technique). These photographs provide sufficient resolution to record the occurrence and types of structures that compose the fault and damage zone. We mapped deformation bands, zones of deformation bands and associated slip surfaces, jointed deformation bands, joints, sheared joints, fragmentation and breccia zones, and fault rock. Structure frequency and orientation were measured along scan lines normal to the faults. We present the least complicated faults first, beginning with the Glass and La Sal faults, and then move on to the more complicated examples of the North and Cottonwood faults (Fig. 2).

3.1. Structures composing WNW-striking faults

Along the Glass fault (Fig. 2), joints are the dominant structural components. The trace of the fault is characterized by a zone of high joint density (Figs. 4 and 5). The upper and lower tips of joints

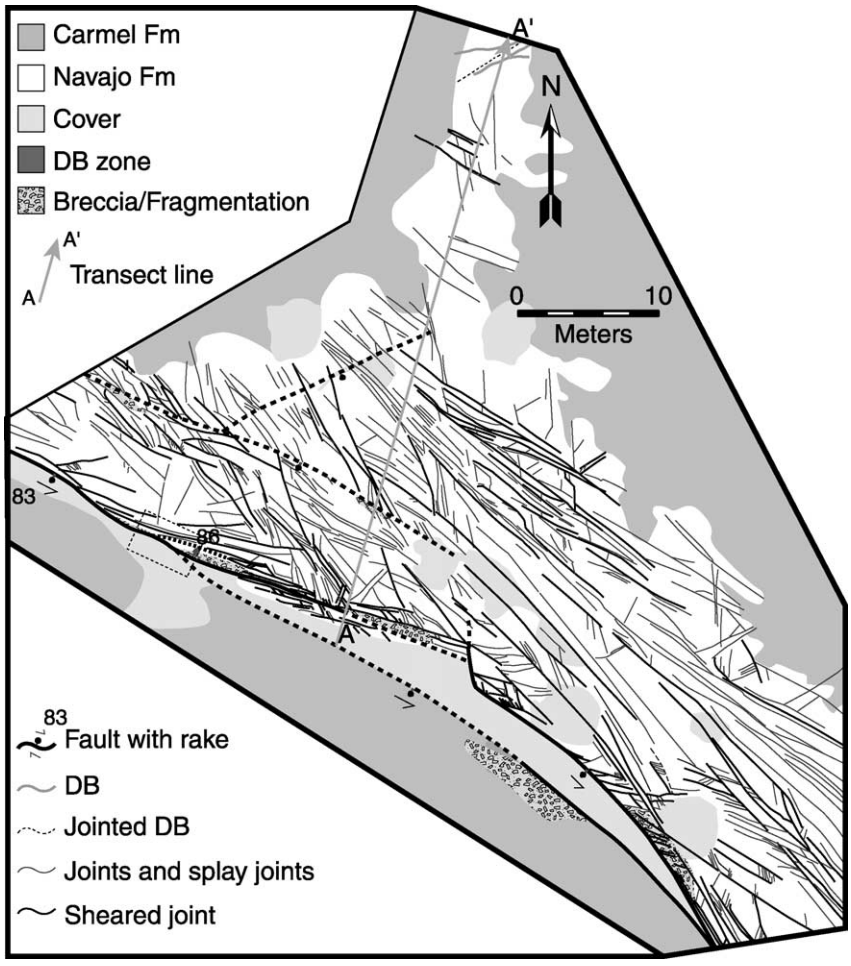

Fig. 5. Detailed map of portion of the Glass fault, offset in this location is approximately 36 m. The fault is principally composed of joints. Only three deformation bands were mapped at the northern extremity of the map. Figure location is indicated in Fig. 2.

typically abut against cross-bedding or dune-bounding surfaces. Some joints have preserved plumose surface morphology (Pollard and Aydin, 1988). Other discontinuities of the same orientation have normal displacements of 0.5–5 cm, implying that joints formed and were subsequently sheared. Younger joints typically abut these sheared joints in a geometry and sense of shear consistent with splay joints (Figs. 1b and 4a).

Near the fault surface, some joints with splay joint geometry accommodate shear offset. These sheared splay joints also have abutting joints in splay joint geometry. Fault surfaces that accommodate offset greater than 1 m are consistently bordered by white fault rock that is surrounded by breccia and fragmented rock (Fig. 4b). Breccia blocks are bounded by sheared joints and joints. The density of joints is lower at the margins of the breccia zone where some of these joints are identifiable as splay joints from the age relationship, sense of shear across the sheared joint, and geometry. Several discontinuous and subparallel fault surfaces bordered by breccia and zones of fault rock are typically present along the Glass fault (e.g., Fig. 5). A single, continuous fault surface is exposed for 10 m along the wall of a mineshaft (location in Fig. 2). This fault surface is bordered by a continuous zone of fault rock. The fault juxtaposes Navajo sandstone against Carmel Formation shale indicating offset greater than 20 m.

The La Sal fault is one of the WNW-striking faults, but in contrast to the Glass fault, it dips to the NNE (Fig. 2). The fault zone is composed of joints (Fig. 4b and c), sheared joints, and associated splay joints similar to those described along the Glass fault. Other faults in the WNW-striking pair of sets share this architecture regardless of dip direction (Fig. 2). In all cases, joint density is highest around the WNW-striking faults consistent with the inferred deformation mechanism (Fig. 6). Deformation bands parallel to the WNW-striking fault sets are rare. When deformation bands are present, they occur at the background density, are not adjacent to the primary fault surface, and are not continuous along the fault. Where deformation bands are present, they are always cut by joints and sheared joints indicating that joints are younger.

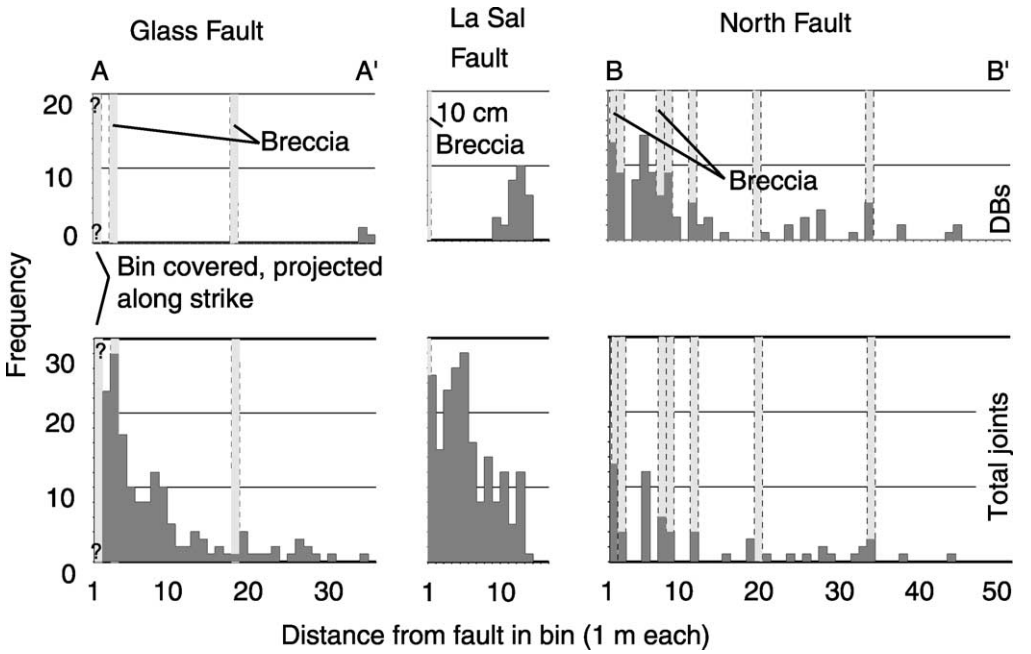

Fig. 6. Frequency of deformation bands (DBs) and all structures formed as joints (e.g., joints, sheared joints, and splay joints) along transects normal to the trend of the Glass (Fig. 5), La Sal, and North (Fig. 8) faults. Transects are indicated in Figs. 5 and 8. Gray bins include slickensided faults.

3.2. Regional joint sets

Joints also occur throughout the field area. Three distinct regional joint sets (Fig. 7a) are recognizable at a distance from faults in the field area. All of the joint sets dip approximately 90°. These joints are primarily exposed in pavement surfaces of thin limestone beds within the overlying Carmel formation. The three joint

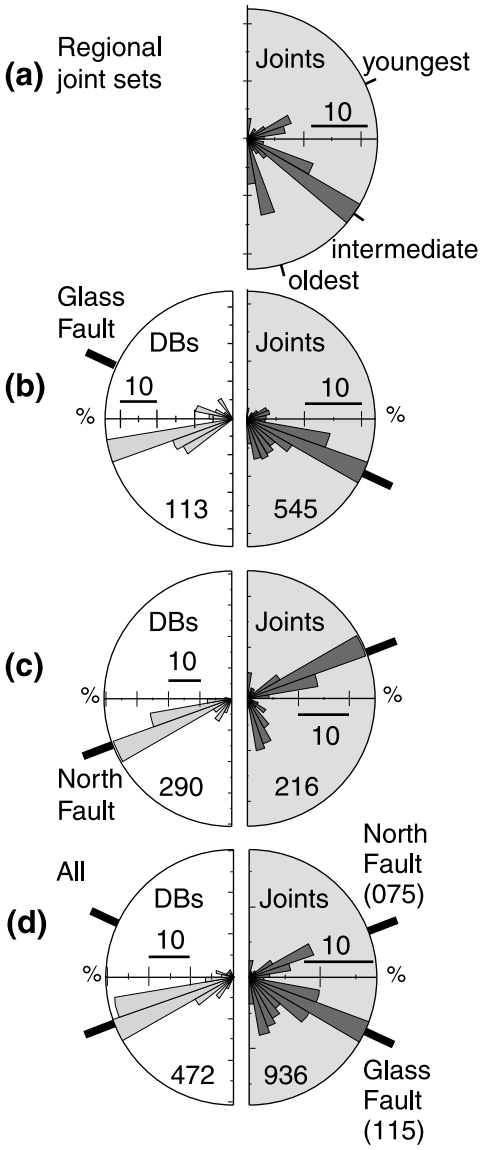

Fig. 7. Strike of deformation bands and joints in Navajo sandstone for (a) joints distant from faults, (b) Glass fault, (c) North fault, and (d) all measurements in the field area including measurements distant from faults. A low density of WNW- and ENE-striking deformation bands is found throughout the field area.

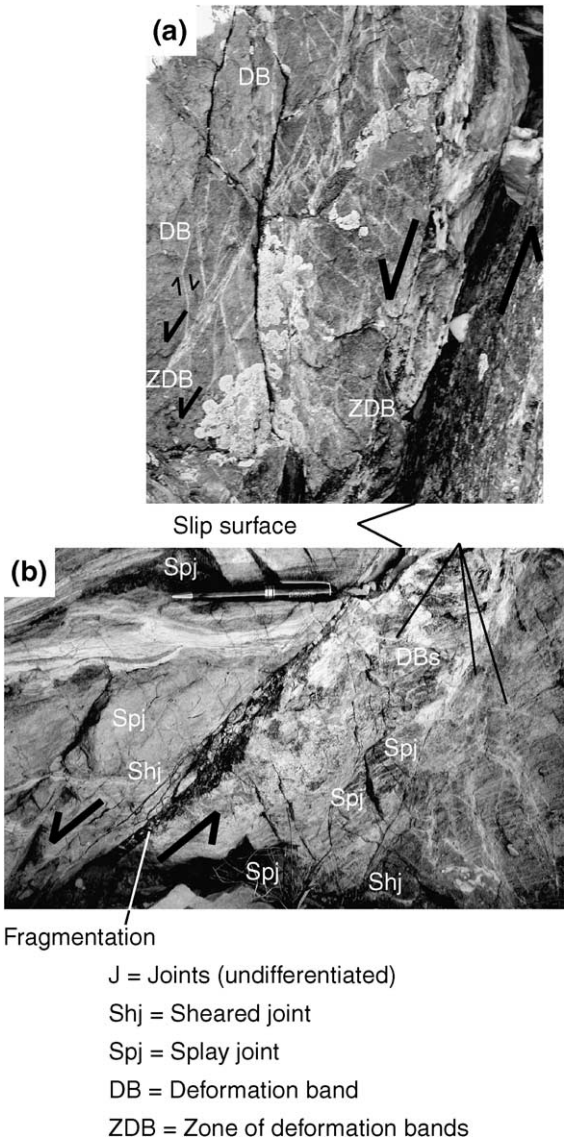

Fig. 8. Components of ENE-striking faults: (a) Well-developed zone of deformation bands (DBs) (lighter colored bands) with adjacent slip surface along the North fault; vertical offset is about 20 m in this location. (b) Zone of deformation bands with slip surface is overprinted by splay joints on the Cottonwood normal fault; vertical offset is about 6 m in this location. Note that joints are oblique to the outcrop surface; thus intersection angles appears larger than they are. Several examples of each structural component are indicated in the photographs. Figure locations are indicated in Fig. 2.

sets also appear to exist in limited exposures of the Navajo sandstone distant from the faults. Consistent relative ages between the joint sets are evident from abutting relationships. The most prominent set of joints strikes 110–140° (Fig. 7a) parallel to the WNW-striking faults (Fig. 7b) and is intermediate in age. The oldest and youngest joint sets oriented from 160° to 180° (Fig. 7a) and from 050° to 080°, respectively, are less prominent. Joints in the oldest two sets were subjected to a small degree of shearing evident from offset markers. The presence of WNW-striking regional joints is consistent with development of WNW-striking faults by shearing along the joints.

3.3. Structures composing ENE-striking faults

Both deformation bands and spatially associated joints are distributed along the entire length of the North fault (Fig. 2). Deformation bands, zones of deformation bands, and slip surfaces adjacent to some of the deformation band zones (Fig. 8a) constitute the majority of structures along the North fault (Figs. 6 and 8). These structures were produced by the deformation banding mechanism (Fig. 1a).

Joints along the North fault typically occur adjacent to deformation bands (Fig. 9); some retain plumose structure confirming they formed as joints. Joints are typically straighter than deformation bands and cut adjacent subparallel but wavy bands indicating that they are younger. Some joints adjacent to deformation bands have several centimeters of offset across the fracture surface indicating reactivation in shear. Single deformation bands in the area consistently have 0.5–5 mm normal offset. The additional offset across jointed deformation bands results from shearing across the joint plane.

Some joints are at angles of 20–40° to the primary slip surface of the North fault. These joints characteristically abut against the slip surface and are arranged in a geometry consistent with splay joints for the observed sense of slip. Where the density of these joints is high, they define rock fragments ranging in

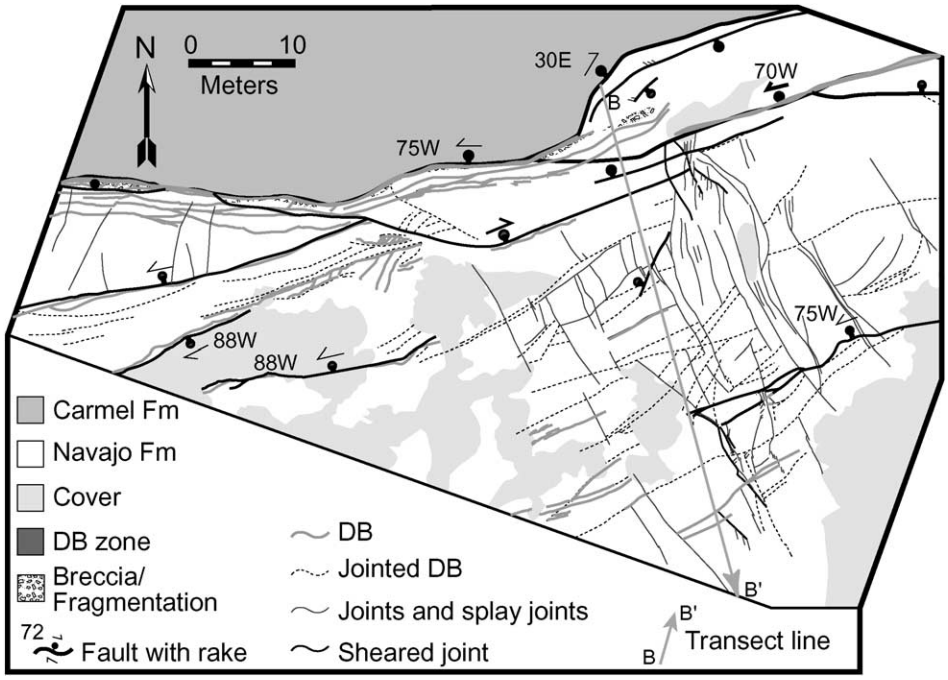

Fig. 9. Detailed map of portion of the North fault, vertical offset in this location is approximately 22 m. The fault is composed of deformation bands cut by joints and splay joints consistent with both the deformation banding and joint-based mechanisms. Figure location is indicated in Fig. 2.

size from centimeters to about 1 m forming a weakly defined breccia, similar to those along the Glass fault. Some joints parallel to the fault may also have formed as part of the youngest regional joint set, which has similar strike (Fig. 7a).

The Cottonwood fault, another ENE-striking normal fault in the study area, (Fig. 2) provides one of the best examples of overprinted faulting mechanisms (Fig. 8b). The fault strikes 253° and dips 70–75°, with approximately 6 m of vertical offset at the location of Fig. 8. The Cottonwood fault is composed of a well-developed zone of deformation bands and associated slip surface. The zone of deformation bands is cut by joints that strike parallel to the fault but dip between 50° and 90° in a direction opposite to that of the fault (Fig. 8b). Joints of this orientation are more abundant close to the fault (e.g., Fig. 6) and abut against the fault slip surfaces. The geometry of these joints and sense of offset that they indicate are consistent with formation by splay jointing. At the intersection of the joints with the deformation band slip surface, increased fracture density fragmented the rock forming a weakly defined breccia (Fig. 8b). Similarly, joints subparallel to deformation bands demonstrate slip (Fig. 8b to the right of the deformation band zone) and have associated splay joints.

Opening of splay joints that truncate against the fault surface requires a small amount of offset across the Cottonwood fault surface accompanying joint formation. Because joints cut deformation bands, this slip postdated deformation band formation. Similarly, the occurrence of breccia overprinting deformation bands indicates a magnitude of slip large enough to lead to fragmentation and breccia formation by splay jointing and shearing (Fig. 1b). A meter or more of offset is estimated to be consistent with the breccia formation. Thus, we partition the slip into two phases: 5 m of the total offset was accommodated during deformation band formation and 1 m of offset associated with additional slip across the original slip surface that produced splay joints and breccia. There may be a small contribution to the slip budget by shearing of a few regional joints from the ENE-striking set.

Deformation band density is greatest near the primary fault slip surface and quickly drops to a background density of less than one band/4 m about 45 m away from the fault (Fig. 6). In all cases observed, joints cut deformation bands indicating that joints and joint-related structures are younger.

3.4. Quantitative analysis of fault structural components

The occurrence of structural components and fault architecture described along the North, Cottonwood, Glass, and La Sal faults were compared to all other major faults exposed in the region (Fig. 2). ENE-striking faults are consistently dominated by deformation bands and associated slip surfaces. In Contrast, WNW-striking faults are consistently dominated by joints, sheared joints, zones of fragmented rock, breccia, and fault rock. In addition, there exist regional joints sets and background deformation bands that strike subparallel to faults throughout the Chimney Rock area (Fig. 7). Deformation bands that strike ENE are consistently cut by a small number of deformation bands that strike WNW (Shipton and Cowie, 2001). The deformation banding and joint-

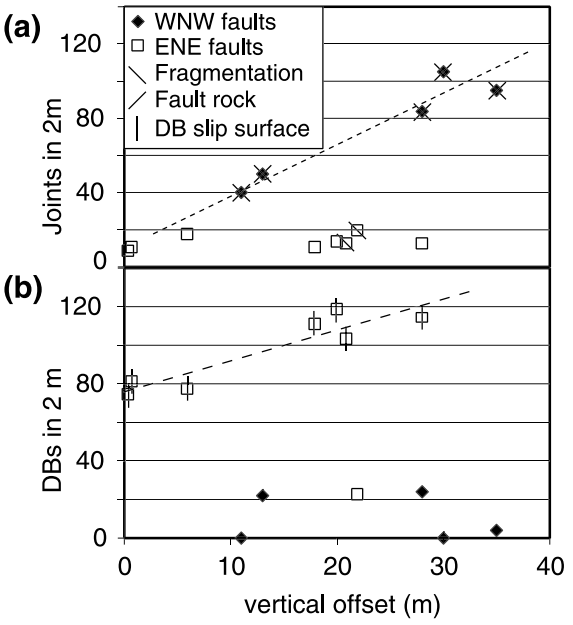

Fig. 10. Vertical offset versus (a) number of joints and (b) number of deformation bands within 2 m of fault slip surface. Data were collected from different locations along single faults as well as several different faults. Associated structures such as fragmentation, deformation band slip surfaces, and fault rock related to joint-based faulting are also indicated.

based faulting mechanisms each occur in faults dipping north and south.

Fault development was investigated by measuring the total number of joints and deformation bands within 2 m of fault slip surfaces at locations with different offsets. This method provided a means to evaluate how individual structural components are added as a function of fault slip. The window of observation was chosen as a practical means of gathering data from a wide range of faults and fault offset despite limited exposure. The short distance also allowed us to avoid fault intersections, where the

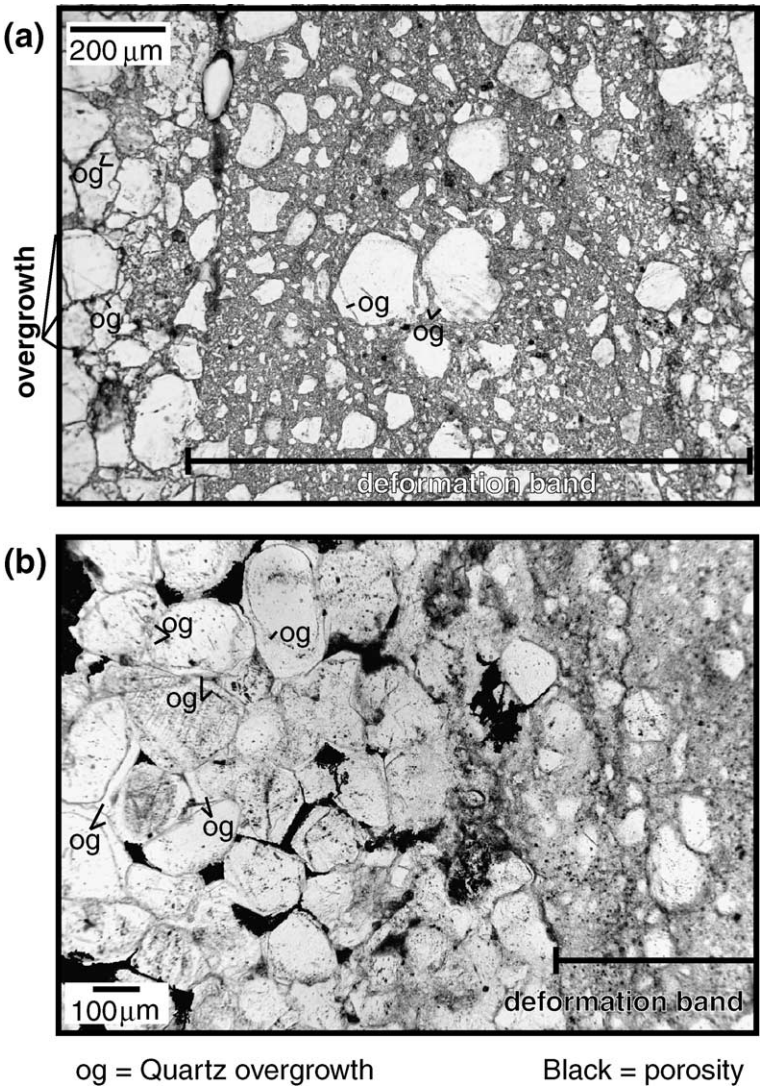

Fig. 11. Photomicrographs in plane-polarized, transmitted light of Navajo formation sandstone showing (a) quartz overgrowth on sand grains in a deformation band as well as (b) quartz overgrowth in the host rock near a deformation band. The tight, angular geometry of overgrowths on intact well-rounded sand grains typical of eolian deposits indicate they are diagenetic rather than inherited. Porosity was digitally enhanced for clarity.

relationship between offset and fault structure is more complicated. A 2-m interval is wide enough to characterize changing deformation intensity within and immediately adjacent to the fault zone based on observations from longer scan lines. Finally, this measurement is consistent with the hypothesis that both zones of deformation bands and joints as splay joints form adjacent to the fault due to continued slip (Aydin and Johnson, 1978; Myers, 1999).

We sampled from multiple locations along the North and Glass faults, as well as several faults with small maximum offsets to assemble a representative database of faults and their architecture. The density of joints (including splay joints) on WNW-striking faults increases with increasing offset (Fig. 10a). In contrast, ENE-striking faults have a consistent density of joints over offsets ranging from 45 cm to 28 m. While deformation band density increases with increasing offset on ENE-striking faults, WNW-striking faults have low or null deformation band density. Fault rock and breccia are developed along WNW-striking faults at all offsets plotted in Fig. 10; fault rock characteristic of joint-based faulting is absent along ENE-striking faults. Conversely, slip surfaces associated with deformation band faults occur along all ENE-striking faults in Fig. 10 beginning at offset as small as 45 cm. The type of slip surface associated with deformation band zones is not observed along WNW-striking faults at any offset. There are, of course, fault planes along WNW-striking faults but these formed by shearing of joints and the related products.

3.5. Fault formation and silica cementation

Sand grains in the Navajo Formation are cemented by quartz overgrowths (Fig. 11). These overgrowths are incorporated into deformation bands (right hand side of Fig. 11) suggesting silica precipitation began before or while the deformation bands formed. Areas of intensely silica-cemented sandstone are localized along some portions of the North and Cottonwood faults implying these faults were partially established prior to and influenced silica cementation. In contrast, joints associated with these faults and at the intersection between the Cottonwood and Glass faults are open and free of silica precipitation and therefore postdate silica cementation of the sandstone.

4. Discussion

4.1. The faulting mechanisms

The structural components observed in the WNW-striking Glass and La Sal faults, their arrangement (Figs. 4–6), the relationship between offset and joint density (Fig. 10), and the WNW-striking regional joint set are consistent with formation by the joint-based faulting mechanism (Fig. 1b). In contrast, the prevalence of deformation bands along the ENE-striking North and Cottonwood faults (Figs. 6 and 8) and the relationship between deformation band density and offset (Fig. 10) indicate that these faults formed by deformation banding (Fig. 1a). Joints are consistently younger than deformation bands on these two faults. In addition, the occurrence of sheared joints, splay joints, and breccia characteristic of joint-based faulting indicate that the North and Cottonwood faults were later reactivated and the additional deformation was accommodated by this mechanism (Fig. 1b). The uniform density of joints along these faults is consistent with a small, comparable contribution to slip by the sheared joint-based faulting mechanism resulting in splay joints (Fig. 10). These joints are superimposed on earlier deformation band faulting that accommodates the majority of slip.

Offset across the ENE-striking North fault results from the combined contributions of both deformation mechanisms. The occurrence of breccia but lack of appreciable fault rock suggests that the overall contribution to slip by shearing across joints is probably no more than 1–2 m (Fig. 1). Rock fragments are isolated from the surrounding rock by joints, but are not yet rotated or entrained and transported significantly along the fault. The minimum offset associated with fragmentation is therefore related to the aperture and density of joints in the fragmentation zone (Fig. 1b). Brecciation requires larger rotation and transport of rock, and thus it is associated with larger offset. Total offset in the mapped location is 22 m; this suggests that at least 20 m of offset was achieved through formation of deformation bands and offset across the associated slip surfaces. The structural components and their arrangement along the North fault require (1) formation of deformation bands, (2) formation of joints adjacent to a preexisting deformation band, (3) formation of joints as splay joints associated with slip on fault

parallel joints and on slip surfaces that formed earlier by the deformation banding mechanism.

4.2. Development of the Chimney Rock fault array

The relative ages of structures produced by each mechanism imply two phases of faulting characterized by different deformation mechanisms. The first phase of faulting was characterized by deformation bands. Subsequently, the second phase of faulting was predominantly characterized by joints, sheared joints, and related splay joints. Early deformation band formation produced principally ENE-striking map-scale faults. After the first phase of faulting, the formation of regional joint sets marked a change in deformation mechanism. Furthermore, the set of WNW-striking joints provided discontinuities that localized shearing leading to the formation of WNW-striking faults. The overprinting of ENE-striking faults is manifested as shearing of deformation band slip surfaces producing splay joints and related products. Additional overprinting might result from shearing of ENE-striking joints formed along deformation bands or by shearing of the regional ENE-striking joint set.

Each deformation mechanism during each respective phase of development caused the formation of faults up to 6 km long with 30–40 m maximum offset. The relative timing and orientation of structures composing the faults suggest that the incremental strain history of the fault array was non-coaxial. The first phase accommodated dominantly NNW extension normal to the two early sets of ENE-striking deformation band faults (Fig. 12). This was followed by the second phase of faulting in which the extension direction was dominantly NNE, normal to the set of WNW-striking joints and subsequent sheared joint based faults. Sometime during this second phase, ENE-striking faults were reactivated. Several lines of evidence, though not conclusive, are consistent with the hypothesis that all sets of faults slipped simultaneously for some portion near the end of the second phase of deformation. First, joints, sheared joints, and fragmentation similar to WNW-striking faults overprint deformation bands on ENE-striking faults along the slip surface. Second, the rake of

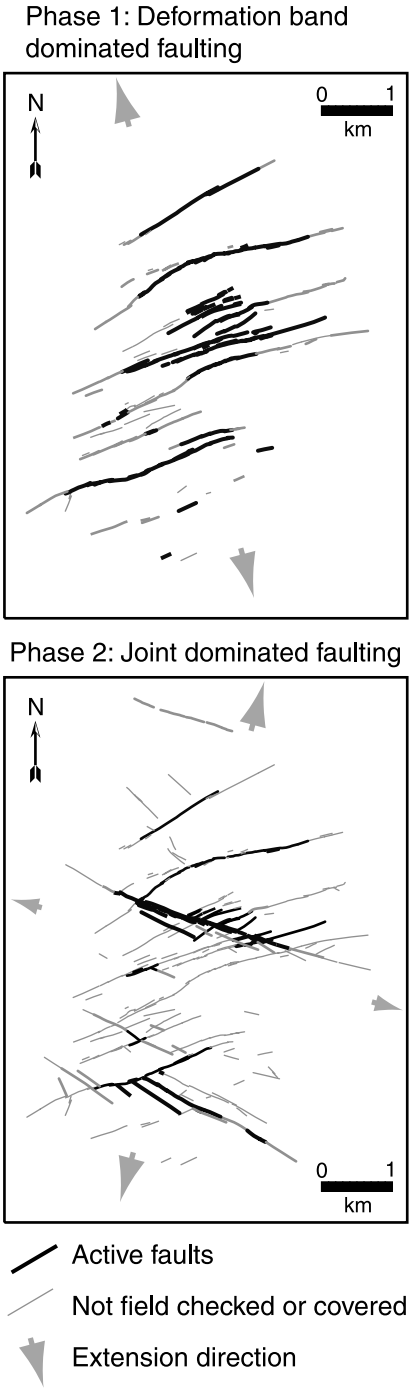

Fig. 12. Two phases of faulting: (1) Faulting characterized by formation of deformation bands and slip surfaces in primarily two conjugate sets, (2) faulting characterized by formation and subsequent shearing of joints in two conjugate sets after rotation of the primary extension direction. As all faults slip, a small amount of extension also occurs to the ESE.

slickensides composing faults throughout Chimney Rock rotates in proximity to fault intersections, indicating mechanical interaction among sets of faults (Maerten, 2000).

Previously, four fault sets with this geometry have been interpreted to have formed simultaneously in response to general three-dimensional strain (Oertel, 1965; Aydin and Reches, 1982; Krantz, 1988). Krantz's (1988) analysis derived the principal strain ratios and orientations based on the fault geometry, spacing, and offset distributions. His analysis assumed coeval fault formation and uniform slip rate on all fault sets resulting in coaxial strain. Multiple phases of fault development were not distinguished. This study indicates that formation of fault sets of different strike was not coeval. In fact, ENE faults were reactivated during the second phase of faulting that produced WNW-striking faults. The two phases of faulting distinguished by the fault architecture in this study suggests non-coaxial strain. During the first phase, the array accommodated predominantly plane strain (Fig. 12). In contrast, during the second phase, the array accommodated three-dimensional strain since all the faults sets were active (Fig. 12). This reconstruction may only be consistent with the rake data that indicate systematic change of slip direction with respect to the fault intersections (Maerten, 2000) and that most likely represent the last phase of slip on the faults. Thus, the previous analyses quantify the finite strain and the kinematic indicators of the last slip events but do not account for sequential fault formation and non-coaxiality in the strain path.

The relative contributions of each deformation mechanism to accommodation of offset controls the overall fault architecture including density, geometry, and type of fault zone components such as joints or deformation bands (Fig. 10). Even at low offset, faults formed from joints define a wide zone of well-connected fractures with initially discontinuous fault rock pockets (disaggregated white gouge). Joint density increases proportionally with increasing fault offset as splay fractures form accompanying slip. These joints and their shearing occurred preferentially along older deformation bands thus contributing to the further development of ENE faults. Along an established fault surface, the offset required to form splay joints might depend on the size of the sliding surface, the stiffness, and frictional properties of the rock (Cruikshank et al., 1991; Willemse and Pollard, 1998). Once slip occurs, many splay joints may form in a wide area around the slipping fault. Deformation band faults tend to develop tightly clustered zones of deformation bands adjacent to the primary fault surface at offsets as low as ~ 0.5 m. As offset increases, a discrete slip surface forms and subsequently new deformation bands.

Fossen and Hesthammer (1997) and Shipton and Cowie (2001) observed a similar relationship between fault offset and damage zone width in faults composed of deformation bands and the associated slip surfaces on the Colorado Plateau. They document large increases in fault damage zone width with very small increases in offset followed by smaller increases in damage zone width per additional unit offset once the fault reaches a few meters of offset. They associated the decrease in damage zone expansion with offset with the development of a through-going slip surface. Cowie and Shipton (1998) offer an alternate interpretation for a similar relationship based on examination of the Blueberry fault (Fig. 2) and the Big Hole fault south of Chimney Rock. They suggested that the decrease in damage zone expansion resulted from a transition from the interior of the fault to the fault tips and related to fault propagation.

In general, results from this study indicate that the addition of new structural elements to the fault is a function of offset for both deformation band faults and joint-based faults (Fig. 10). However, on a plot of offset versus structure density, the slope is different for each mechanism. This implies that a clear relationship between fault zone characteristics like fault rock thickness or damage zone width may not exist if more than one mechanism contributes to fault development. In addition, faults with the same offset or length will have very different fault architecture if they form by different deformation mechanisms.

4.3. Primary controls on deformation mechanisms

The deformation banding mechanism is controlled by material properties at the grain scale including porosity, sorting, and composition (Dunn et al., 1973; Antonellini et al., 1994) and the state of stress (Wong et al., 1997). In contrast, shearing of planar discontinuities is controlled by the presence of macroscopic flaws (e.g., joints, dune boundaries, pre-existing fault

surfaces) in a favorable orientation to localize shear stress (Brace and Bombolakis, 1963; Segall and Pollard, 1983; Cooke, 1997). The formation of deformation bands during early phases of faulting establishes an anisotropy that is exploited by subsequent shearing along joints (Cruikshank et al., 1991; Antonellini and Aydin, 1995). This may explain why joints close to ENE-striking faults are parallel to the fault rather than the WNW-striking set. Another possibility is that the stress field perturbed by the nearby slipping fault controlled the orientation of joints (Peacock, 2001; Bourne and Willemse, 2001).

Joints occupy a principal plane normal to the least compressive stress during fracturing (Pollard and Aydin, 1988). In order for joints to slip, shear stresses must resolve on the joint plane and their magnitude must exceed the frictional strength of the joint surfaces. Shear stresses on the fracture plane can result from either stress or material rotation. Dyer (1983) and Cruikshank et al. (1991) recognized a complex stress history characterized by rotation of the stress field following joint formation leading to shearing of the joints. In contrast, Peng and Johnson (1972) advanced a conceptual model for failure of a granite specimen in a triaxial deformation experiment on granite. Failure begins with formation of closely spaced en echelon joints. These joints define individual rock ‘‘beams’’ that subsequently rotate and fail by slipping and forming connecting splay joints. This model does not require rotation of the far-field stress. Finally, the presence of some deformation bands and the observation of joints along deformation bands associated with WNW-striking faults suggest that the deformation bands may have contributed to the formation of some early joints slightly out of line with respect to the regional stress field (Cruikshank et al., 1991; Antonellini and Aydin, 1995).

It is unlikely that single joints span the more than 140 m thickness of the Navajo sandstone. Joints of varying height controlled by cross-bedding, dune-bounding surfaces, and other structures are most likely distributed throughout the thickness. As a result, the manner in which joints are sheared and linked by splay joints ultimately controls the dip direction of the resulting fault analogous to rock mechanics experiments (Peng and Johnson, 1972). Similarly, the opportunity to form an extensive network of sheared joints may be the primary control on the spacing of WNW faults. This process also leads to the elevated joint density near faults as splay joints are formed accompanying slip. The locally increased joint density, fragmentation, breccia, and fault rock are radically different than those of ENE faults characterized by deformation bands.

Formation of quartz overgrowths on sand grains is commonly observed at temperatures greater than 90 to 100 °C (Bjørlykke and Egeberg, 1993) in quartz rich sandstones such as the Navajo Formation. If temperature is controlled by burial, a normal geothermal gradient of 30 °C/km requires 3 km of overburden to achieve well-developed quartz overgrowth. Because deformation band formation overlaps with silica cementation this empirical relationship suggests that deformation bands developed at or near the maximum burial of the Navajo sandstone achieved during the Laramide Orogeny (Fig. 3).

The transition between deformation mechanisms may be initiated by a change in rheology or deformation environment or both. A change in rheology may accompany cementation (Dvorkin and Nur, 1996). An increase in cement and loss of pore space could render the deformation banding mechanism unfavorable (Aydin and Johnson, 1978; Antonellini et al., 1994). Hence, continued silica precipitation may have been a key cause of the change in faulting mechanism. In addition, deformation bands generally form under compressive differential stresses (Wong et al., 1997; Mair et al., 2000) whereas joints require effective tensile stress to form. A change in the deformation environment, such as the state of stress or pore fluid pressure, could cause a transition from deformation banding to jointing. The inference that deformation banding develops at conditions close to the maximum burial depth might also suggest that the transition to joint formation coincided with the onset of exhumation.

4.4. Implications for faults and fluid flow

Changing fault architecture between deformation phases has a potential impact on the ability of a fault to act as a fluid conduit or a barrier. The effects of a fault on subsurface fluid flow results from the type of structures composing the fault, their distribution, and connectivity (Caine et al., 1996; Knipe et al., 1998; Myers, 1999; Taylor et al., 1999; Aydin, 2000). How

and what elements are added during fault development is a function of deformation mechanism and will control the permeability behavior of the fault through time. Joints and slightly sheared joints are potential fluid conduits enhancing fluid flow parallel to the joint (Taylor et al., 1999). Along faults formed by shearing of joints and the attendant products (the WNW-striking faults in this study), fault parallel permeability is greatly increased whereas fault normal fluid flow is reduced after a few meters of slip as continuity of fault rock develops (Flodin et al., 2001; Jourde et al., 2002). Deformation bands inhibit fault normal fluid flow due to the porosity reduction in the band (Antonellini et al., 1994; Matthai et al., 1998). Furthermore, each mechanism is distinguished by the number of structures accrued with offset. A dense network of deformation bands will form with only small slip, whereas joints easily cut and breach deformation bands. The overprinting of these two deformation products will result in a change of permeability behavior over time from primarily sealing to largely conduit.

5. Conclusions

We have identified the structural components of multiple fault sets in Chimney Rock, San Rafael Swell, Utah, USA. The structural components are organized into two distinct fault architectures characteristic of faults formed by (1) deformation bands and (2) by shearing of joints and associated splay jointing. The distribution of structures produced by these deformation mechanisms, their relative intensity, and their temporal evolution allow us to partition the deformation into two phases of faulting that could not be distinguished based on the map-scale fault pattern alone. The earlier phase involves deformation band faults comprising two oppositely dipping sets striking ENE–WSW and minor development of faults striking WNW–ESE. The later phase of joint-based faulting dominates fault development along WNW–ESE faults and makes a minor contribution to ENE–WSW faults. In summary, what appears to be nearly homogeneous three-dimensional, fault-related strain field was actually produced by two phases of faulting reflected by a change in deformation mechanism. The juxtaposition of both deformation mechanisms along two well-defined pairs of fault sets with common strike direction suggests that faults of different architecture can develop within a single rock type at the same locality. We have demonstrated that faults with the same geometric characteristics of length and offset in a single rock type and locality can have radically different fault architecture. The earlier faults composed of deformation bands were probably sealing for fluids. In contrast, later faulting probably established higher permeability pathways because of joint development and joints intersecting deformation bands, thereby negating the sealing effect of the older faults.

Acknowledgements

This work greatly benefited from support by several individuals. Laurent Maerten shared maps, data, and advice produced during his own work in the Chimney Rock fault array. Bob Krantz, Mary Beth Gray, and Phil Resor critically reviewed the manuscript during its development and provided useful and candid advice. Nick Davatzes would also like to acknowledge the helpful environment and financial support provided by the Rock Fracture Project that contributed to the completion and quality of this work. We thank Terry Engelder and Zoe Shipton for their constructive reviews that helped to improve the manuscript.

References

Anderson, E.M., 1951. The Dynamics of Faulting and Dyke Formation with Applications to Britain. Oliver & Boyd, Edinburgh. 206 pp.

Antonellini, M., Aydin, A., 1995. Effect of faulting on fluid flow in porous sandstones; geometry and spatial distribution. Am. Assoc. Pet. Geol. Bull. 79, 642–671.

Antonellini, M.A., Aydin, A., Pollard, D.D., 1994. Microstructure of deformation bands in porous sandstones at Arches National Park, Utah. J. Struct. Geol. 16, 941–959.

Aydin, A., 2000. Fractures, faults, and hydrocarbon entrapment, migration and flow. Mar. Pet. Geol. 17, 797–814.

Aydin, A., Johnson, A.M., 1978. Development of faults as zones of deformation bands and as slip surfaces in sandstone. Pure Appl. Geophys. 116, 931–942.

Aydin, A., Reches, Z., 1982. Number and orientation of fault sets in the field and in experiments. Geology 10, 107–112.

Barnett, J.A.M., Mortimer, J., Rippon, J.H., Walsh, J.J., Watterson, J., 1989. Displacement geometry in the volume containing a single normal fault. Am. Assoc. Pet. Geol. Bull. 71, 925–937.

Bjórlykke, K., Egeberg, P.K., 1993. Quartz cementation in sedimentary basins. Am. Assoc. Pet. Geol. Bull. 77, 1538–1548.

Bourne, S.J., Willemse, E.J.M., 2001. Elastic stress control on the pattern of tensile fracturing around a small fault network at Nash Point, UK. J. Struct. Geol. 23, 1753–1770.

Brace, W.F., Bombolakis, E.G., 1963. A note on brittle crack growth in compression. J. Geophys. Res. 68, 3709–3713.

Caine, J.S., Evans, J.P., Forester, C.B., 1996. Fault zone architecture and permeability structure. Geology 24, 1025–1028.

Chester, F.M., Logan, J.M., 1986. Implications for mechanical properties of brittle faults from observations of the Punchbowl Fault Zone, California. Pure Appl. Geophys. 124, 79–105.

Cooke, M.L., 1997. Fracture localization along faults with spatially varying friction. J. Geophys. Res. 102, 22425–22434.

Cotterell, B., Rice, J.R., 1980. Slightly curved or kinked cracks. Int. J. Fract. 16, 155–169.

Cowie, P.A., Shipton, Z.K., 1998. Fault tip displacement gradients and process zone dimensions. J. Struct. Geol. 20, 983–997.

Cruikshank, K.M., Aydin, A., 1994. Role of fracture localization in arch formation, Arches National Park, Utah. Geol. Soc. Am. Bull. 106, 879–891.

Cruikshank, K.M., Zhao, G., Johnson, A.M., 1991. Analysis of minor fractures associated with joints and faulted joints. J. Struct. Geol. 13, 865–886.

Dawers, N.H., Anders, M.H., 1995. Displacement–length scaling and fault linkage. J. Struct. Geol. 17, 607–614.

Dickinson, W.R., Snyder, W.S., 1978. Plate tectonics of the Laramide Orogeny. Geol. Soc. Am. Mem. 151, 355–366.

Dunn, D.E., LaFountain, L.J., Jackson, R.E., 1973. Porosity dependence and mechanism of brittle fracture in sandstones. J. Geophys. Res. 78, 2403–2417.

Dvorkin, J., Nur, A., 1996. Elasticity of high-porosity sandstones: theory for two North Sea data sets. Geophysics 61, 1363–1370.

Dyer, J.R., 1983. Jointing in Sandstones, Arches National Park, Utah. PhD thesis, Leland Jr. Stanford University, Stanford, CA.

Engelder, J.T., 1974. Cataclasis and the generation of fault gouge. Geol. Soc. Am. Bull. 85, 1515–1522.

Engelder, J.T., 1987. Joints and shear fractures in rock. In: Atkinson, B.K. (Ed.), Fracture Mechanics of Rock. Academic Press, London, pp. 27–69.

Flodin, E.A., Aydin, A., Durlofsky, L.J., Yeten, B., 2001. Representation of fault zone permeability in reservoir flow models. SPE paper 71671. SPE Annual Technical Conference and Exhibition, New Orleans, p. 10.

Fossen, H., Hesthammer, J., 1997. Geometric analysis and scaling relations of deformation bands in porous sandstone. J. Struct. Geol. 19, 1479–1493.

Gilluly, J., 1928. United States geology and oil and gas prospects of parts of the San Rafael Swell, Utah. U.S. Geol. Surv. Bull. 806-C, 69–130.

Gilluly, J., Reeside Jr., J.B., 1928. Sedimentary rocks of the San Rafael Swell and some adjacent areas in eastern Utah. U.S. Geol. Prof. Pap. P0150-D, 61–110.

Granier, T., 1985. Origin, damping, and pattern of development of faults in granite. Tectonics 4, 721–737.

Guiseppe, A.C., Heller, P.L., 1998. Long-term river response to regional doming in the Price River Formation, central Utah. Geology 26, 239–242.

Hintze, L.F., 1988. Geologic history of Utah. Brigham Young University Geology Studies Special Publication 7. Brigham Young University, Provo, UT, p. 202.

Huang, Q., Angelier, J., 1989. Inversion of field data in fault tectonics to obtain the regional stress: II. Using conjugate fault sets within heterogeneous families for computing palaeostress axes. Geophys. J. 96, 139–149.

Jourde, H., Flodin, E.A., Aydin, A., Durlofsky, L.J., Wen, X.-H., 2002. Computing permeability of fault zones in aeolian sandstone from outcrop measurements. Am. Assoc. Pet. Geol. Bull. 86, 1187–1200.

Kelley, V.C., 1955. Monoclines of the Colorado Plateau. Geol. Soc. Am. Bull. 66, 789–803.

Knipe, R.J., Jones, G., Fisher, Q.J., 1998. Faulting, fault sealing and fluid flow in hydrocarbon reservoirs: an introduction. In: Knipe, R.J., Jones, G., Fisher, Q.J. (Eds.), Faulting, Fault Sealing and Fluid Flow in Hydrocarbon Reservoirs. Geological Society, London, Special Publications, vol. 147, pp. vii–xxi.

Krantz, R.W., 1988. Multiple fault sets and three-dimensional strain; theory and application. J. Struct. Geol. 10, 225–237.

Krantz, R.W., 1989. Orthorhombic fault patterns; the odd axis model and slip vector orientations. Tectonics 8, 483–495.

Maerten, L., 1999. Mechanical Interaction of Intersecting Normal Faults; Theory, Field Examples and Application. Ph.D. thesis, Leland Stanford Jr. University, Stanford, California. 167 pp.

Maerten, L., 2000. Variation in slip on intersecting normal faults: implications for paleostress inversion. J. Geophys. Res. 105, 25553–25565.

Maerten, L., Pollard, D.D., Maerten, F., 2001. Digital mapping of three-dimensional structures of the Chimney Rock fault system, central Utah. J. Struct. Geol. 23, 585–592.

Mair, K., Main, I., Elphick, S., 2000. Sequential growth of deformation bands in the laboratory. J. Struct. Geol. 22, 25–42.

Martel, S.J., 1988. Formation of compound strike–slip fault zones, Mount Abbot Quadrangle, California. J. Struct. Geol. 12, 869–882.

Martel, S.J., 1990. Formation of compound strike-slip fault zones, Mount Abbot Quadrangle. J. Struct. Geol. 12, 869–882.

Martel, S.J., Pollard, D.D., Segall, P., 1988. Formation of compound strike–slip fault zones, Mount Abbot Quadrangle, California. J. Struct. Geol. 12, 869–882.

Matthai, S.K., Aydin, A., Pollard, D.D., Roberts, S.G., Fisher, Q.J., Knipe, R.J., 1998. Numerical simulation of departures from radial drawdown in a faulted sandstone reservoir with joints and deformation bands. In: Jones, G., Fisher, Q.J., Knipe, R.J. (Eds.), Faulting, Fault Sealing and Fluid Flow in Hydrocarbon Reservoirs. Geological Society, London, Special Publications, vol. 147, pp. 157–191.

Myers, R.D., 1999. Structure and Hydraulics of Brittle Faults in Sandstone. PhD thesis, Leland Stanford Jr. University, Stanford, California. 176 pp.

Oertel, G., 1965. The mechanics of faulting in clay experiments. Tectonophysics 2, 343–393.

Peacock, D.C.P., 2001. The temporal relationships between joints and faults. J. Struct. Geol. 23, 329–341.

Peng, S., Johnson, A.M., 1972. Crack growth and faulting in cylindrical specimens of Chelmsford granite. Int. J. Rock Mech. Min. Sci. 9, 37–86.

Pollard, D.D., Aydin, A., 1988. Progress in understanding jointing over the past century. Geol. Soc. Am. Bull. 100, 1181–1204.

Schlische, R.W., Young, S.S., Ackermann, R.V., Gupta, A., 1996. Geometry and scaling relations of a population of very small rift-related normal faults. Geology 24, 683–686.

Segall, P., Pollard, D.D., 1983. Nucleation and growth of strike slip faults in granite. J. Geophys. Res. 88, 555–568.

Shipton, Z.K., Cowie, P.A., 2001. Analysis of three-dimensional fault zone structures over a micrometer to km scale range in the high-porosity Navajo sandstone, Utah. J. Struct. Geol. 23, 1825–1844.

Taylor, L., Pollard, A., Aydin, A., 1999. Fluid flow in discrete joint sets; field observations and numerical simulations. J. Geophys. Res. 104, 28983–29006.

Willemse, E.J.M., Pollard, D.D., 1998. On the orientation and patterns of wing cracks and solution surfaces at the tips of a sliding flaw or fault. J. Geophys. Res. 103, 2427–2438.

Wong, T.-F., David, C., Zhu, W., 1997. The transition from brittle faulting to cataclastic flow in porous sandstones; mechanical deformation. J. Geophys. Res. 102, 3009–3025.